Heliyon 6 (2020) e03574

Contents lists available at ScienceDirect

Heliyon

journal homepage: www.cell.com/heliyon

Research article

Galactomannan as a new bio-sourced corrosion inhibitor for iron in acidic media

Said Abbout [a,*], Meryem Zouarhi [a], Driss Chebabe [b], Mohamed Damej [a], Avni Berisha [c], Najat Hajjaji [a]

[a] Laboratory of Materials, Electrochemistry and Environment, Team of Corrosion, Protection and Environment, Department of Chemistry, Faculty of Sciences, Ibn Tofail University, BP 133, 14000 Kenitra, Morocco
[b] Laboratory of Natural Substances & Synthesis and Molecular Dynamic, Faculty of Sciences and Techniques, Moulay Ismail University of Meknes, BP 509, 52000, Boutalamine, Errachidia, Morocco
[c] Department of Chemistry, Faculty of Natural and Mathematics Science, Prishtina University, 10000, Prishtina, Kosovo, Serbia

ARTICLE INFO

Keywords:
Electrochemistry
Food science
Corrosion inhibition
HCl Media
Galactomannan
Carob
Electrochemical measurements
Theoretical study

ABSTRACT

The aim of this study is to evaluate the impact of a bio-sourced polymer as a corrosion inhibitor against iron corrosion in a 1 M HCl solution. Galactomannan was obtained from the carob plant (Ceratonia Siliqua L) and its structure was verified by infrared spectroscopy (FTIR) and elemental analysis. The inhibitor concentration effects and immersion time on the resistance of the iron surface against corrosion are evaluated using impedance and polarization electrochemical measurements, UV-visible analysis and theoretical study. The results show that the galactomannan is a mixed type inhibitor act by physisorption and chemisorption on the metal surface. In addition, the efficiency of these compounds increases with increasing the concentration of the inhibitor and reaches a value of 87.72% at a concentration of 1 g/l. The electrode surface was characterized by SEM surface analysis method coupled with EDS.

1. Introduction

The natural substances contain many active compounds, which makes them appropriate for use in different domains, including corrosion inhibition. These substances act either by blocking the active corrosion sites or by forming a film on the metal surface or by forming insoluble complexes on the metallic surface [1, 2, 3, 4].

Recently, the bio-sourced polymer extracted from plants has been the subject of several researches in the field of corrosion inhibition to protect iron in different corrosive media. It was found that these substances have a remarkable inhibiting efficiency. Their usefulness is due to the fact that they are ecological and non-toxic compounds [5, 6, 7].

One of the areas in which green chemistry, often applied to biomass-derived products, offers novelty in terms of reducing negative environmental and waste impacts [8]. Metal material degradation has generally been resolved by the use of environmentally friendly organic compounds. Aggressive solutions, such as acid solution, are widely used in the process industries to take away deposited scales from metal surfaces during the production, procedure and storage phases [9].

In aim to valorize the Galactomannan extract from *Ceratonia siliqua* L, we are used it as a corrosion inhibitor to improve the resistance of the iron, and to minimize the aggressive attack of 1M HCl medium using the electrochemical measurements (polarization measurements and impedance spectroscopy tests) and theoretical study (DFT and molecular dynamic). The protective effect was confirmed by analyzing the surface morphology of iron with and without inhibitor in 1 M HCl solution using the SEM coupled with EDS.

2. Experimental techniques

2.1. Biopolymer extraction from Moroccan carob

The carob used in this study is of Moroccan origin. The pods were crushed, and the seeds were manually separated.

2.1.1. Isolation of the unpurified biopolymer

In order to obtain gum of high quality and white color, an acidic treatment was used for decortication, consisting of maceration of 100 g of H_2SO_4/H_2O sulphuric acid seeds (60%/40%) for 60 min at 60 C in a preheated water bath when regularly stirring [10, 11]. Intensive cleaning

* Corresponding author.
E-mail addresses: Said_about@hotmail.fr, Said.abbout@uit.ac.ma (S. Abbout).

https://doi.org/10.1016/j.heliyon.2020.e03574
Received 2 November 2019; Received in revised form 4 January 2020; Accepted 9 March 2020

and brushing was achieved via a 2 mm metal sieve to avoid the carbonated hull. The dehulled seeds were then soaked overnight in distilled water to enlarge, allowing the germs to be manually isolated from endosperms. They were then washed and dried in the oven at 105 C for 4–5 h, eventually; Endosperms were then milled for the manufacture of raw, unpurified locust bean gum using a laboratory miller. Due to the high temperature increases experienced during the phase, the consistency of powdered, unpurified LBG relies on the milling process that sometimes darkenes the powder. Milling operation determined the size and color of the final product. The color and the size of the particles also indicate impurities [12].

2.1.2. Solubilization of the biopolymer

To control the microbiological of the unpurified powder, it was washed with acetone and ethanol using a sintered (no.3) [13]. Then, 1.3g of unpurified powder was solubilized in 100 ml of distilled water at room temperature for 2 h under gently stirring [14] and kept at 252 K for overnight. Afterward, the solutions were heated at 353 K in water bath for 30 min with continuous agitation. After cooling the solution, a centrifugation step is necessary (1hour, 10000rpm, 253K) in order to eliminate the insoluble matter [15].

The last step was collecting the superior party of the solution, which contains the solubilized biopolymer.

2.1.3. Purification of the biopolymer

The purified galactomannan has been produced by precipitation with isopropanol. Through removing impurities and endogenous enzymes, this procedure removes all unwanted raw LBG flavors and offers a cleaner and more stable solution. Galactomannan was precipitated by pouring more than two volumes of isopropanol from the crude LBG solution allowing the mixture to stand for 30 min. White fibrous matter has been collected and screened through a tube, and isopropanol and acetone washed twice. The resultant friable solid was crushed into a fine powder after a 48-h freeze-drying phase [12].

2.2. Characterization of the Moroccan biopolymer

2.2.1. Elementary analysis

The elemental analysis was performed by using multi EA-5000.

2.2.2. Spectroscopic analysis (FTIR)

Measurements by FTIR were carried out using an FTIR, Bruker Spectrum instrument. The dried polysaccharide was scattered on ATR-A225 diamond. The FTIR spectra (50 scans, 4cm^{-1}resolution) were unregistered at room temperature in the wave-numbers range of 500–4000 cm^{-1} at room temperature.

2.3. Iron chemical composition

The chemical composition (weight percent) of the electrode (coupon iron) is given in Table 1 [3].

2.4. Electrochemical analysis

The electrochemical, analysis was evaluated using a three electrode cell, the working electrode (WE) is an iron disc with a surface area of 1cm^2. The reference electrode is a saturated calomel (KCl saturated) electrode and the counter electrode is platinum.

Each experiment is previous by polishing the working electrode with emery papers of increasing grain size from 600 to 1500 to obtain a smooth and shiny surface. Then, it is cleaned with distilled water and dried with hot air. These analyses were performed using a Potentiostat type Bio Logic SP-200 device controlled by a computer equipped by EC-LAB software [16], the experiments were replicated three times.

The corrosive medium is a 1M hydrochloric acidic, prepared diluted concentrated acid (HCl, 37%) in distilled water.

2.4.1. Potentiodynamic polarization

The WE was immersed in the solution for 0.5 h to reach the equilibrium potential. Then, the anodic and cathodic polarization curves are recorded with 1 mV/s rate scanning. This speed allows getting as close as possible to the steady-state conditions of the studied system.

2.4.2. Electrochemical impedance spectroscopy

The electrochemical impedance spectroscopy (EIS) study was carried out using a 10mV amplitude signals in the frequency spectrum interval from 100 kHz to 0.10 Hz at open circuit potential (OCP).

The recording of EIS spectra begins after 30 min of immersion. Then, the impedance data were analyzed by the EC-LAB software [17].

The following equation was used to determine the inhibition efficiency at various concentrations of the inhibitor:

$$E\ \% = \frac{R_P - R_{P0}}{R_P} \times 100$$

R_P and R_{P0} are the polarization resistances with and without the inhibitor, respectively [18].

2.5. UV-visible analysis

UV-visible analysis of the solution (1M HCl + 1 g/l of the inhibitor) was evaluated to identify the interactions between molecules of inhibitor and the orbits vacates of iron atoms. The spectrum from 200 nm to 800 nm was registered before and after immersion of the sample at 298 K for 48 h using a Jenway ultraviolet-visible spectrophotometer (series 67).

2.6. Surface analysis

The morphology of the working electrode surface was examined with a scanning electron microscope (SEM) model FEA 450 and the surface characterization was evaluated by X-ray flash (model 6130 Bruker brand) with an acceleration voltage of 20 KV. After 24 h of immersion time in the presence and absence of the inhibitor.

2.7. Quantum computation

2.7.1. DFT

In order to investigate the quantum chemical property of the biopolymer, Gaussian 03W software [19] was used to perform the quantum chemical calculations. Geometry optimization and energy calculation were carried out using the Becke-type three-parameter hybrid DFT approach in conjunction with the Lee, Yang and Parr (B3LYP) gaussian blur-corrected correlation function in combination with the 6 311 G (d, p) base set [20].

2.7.2. DMol3 method

The optimization of structure the inhibitor molecule was carried out using the DMol3 method (by Materials Studio version 2017 software, noted MS2017).

Table 1. The iron substrate Chemical composition used in this study.

Elements	Si	Mn	C	P	S	Fe
W_t %	0.2	0.519	0.157	0.007	0.009	Balance

Table 2. Molecular dynamics simulation conditions.

Plane	Thickness	Mille	Number of water molecules	Simulation time at 298 °K	NVT assembly and COMPASS force field
110	15.5 Å	a = b = 37.236 Å, c = 7.155 Å	50	500 ps	

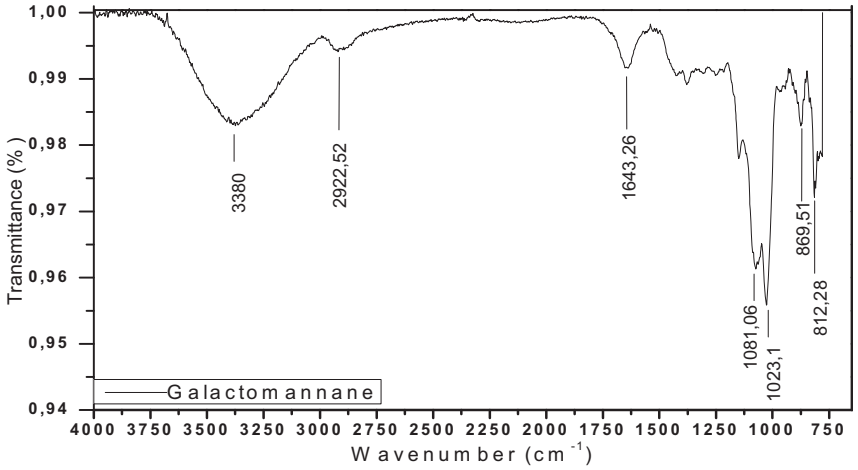

Figure 1. FT-IR spectrum of the Galactomannan extract from the carob seeds.

2.7.3. M D simulation

The quantum simulation of the molecule was performed using a simulation box with periodic limit conditions using MS2017 (Table 2).

Using the adsorption and binding energies calculated by Eqs. (1) and (2), surface metallic-molecule interactions can be evaluated in the simulation system.

$$E_{ads} = E_T - (E_{Su+Sol} + E_{inh+sol}) + E_{sol} \quad (1)$$

$$E_{ads} = E_{bind} \quad (2)$$

with E_T is the total energy of the system and $\mathbf{E_{Su+Sol}}$ represents the total energy of the surface of the Fe_{110} and the solution without inhibitor. On the other hand, $\mathbf{E_{inh+sol}}$ represents the total energy of the Fe surface (Fe_{110}) and $\mathbf{E_{sol}}$ is the energy of the solution without inhibitor.

The Fe_{110} was chosen because it has the lowest surface energy and has more number of adsorption sites. In addition to this, Fe_{110} surface was also chosen as a model for exploring the anticorrosive mechanism of corrosion inhibitors in conventional molecular dynamics simulations [21].

3. Results and discussion

3.1. Biopolymer extraction

The yield of purified galactomannan is 52%. This percentage is important compared to other works. Dakia et al found a yield of 43%, likewise Neukom et al and Herald et al whose performance varied between 42% and 46% with the same shelling method [22]. This gap in yield can be due to the fact that carob biopolymer extraction from whole seeds varies based on the origin of the plants, extraction method, and growing conditions of the carob tree [22].

3.2. Characterization of the biopolymer

3.2.1. Elemental analysis

The elemental analysis shows that the purified biopolymer of the carob tree seeds contains the following atoms oxygen (57.02%), carbon (36.34%), and hydrogen (6.64%). This result is conformed to the galactomannan atoms structure.

3.2.2. Spectroscopic analysis (FTIR)

The Figure 1 illustrates the FTIR spectrum of biopolymer extracts from seeds of Moroccan's carob.

The FTIR spectrum analysis shows the presence of the bond's characteristic functional groups of biopolymer structure:

The presence of an intense wide bonds 3200-3500 cm^{-1} is attributed to the elongation vibration of hydroxyl groups (-OH) which is characteristic of biopolymer as well as to the water absorption [15]. Low bonds of asymmetric vibration of the C–H links are observed between 2800 and 3000 cm^{-1} [11]. In addition, the FTIR spectrum exhibits the presence of characteristic bonds 2800-3000 cm^{-1}, 1550-1650cm^{-1} and 1050-1120cm^{-1} corresponding to the aliphatic, carboxylate function and carbohydrate functions, respectively [23,24]. To the aliphatic function, carboxylate function and carbohydrate function [25].

3.3. Study of the inhibitory effect of biopolymer

3.3.1. Gravimetric measurements

The following histogram presents the evaluation of inhibitor efficiency as a function of the concentration of the inhibitor tested (see the Figure 2).

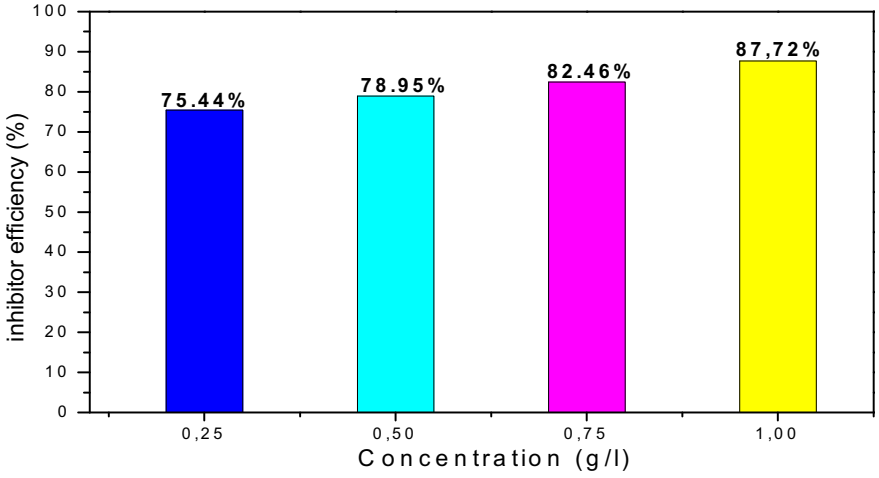

Figure 2. Evaluation of the inhibitor efficiency as a function of the Galactomannan concentration.

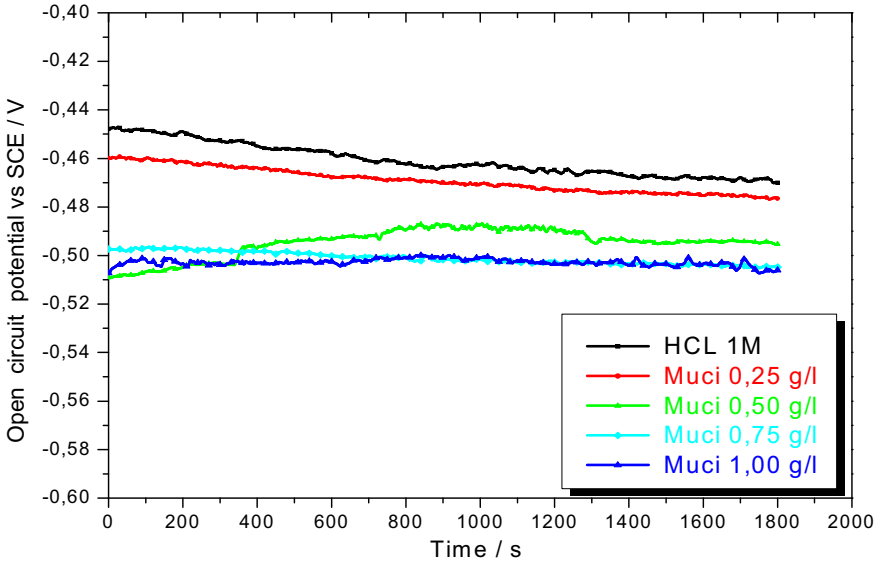

Figure 3. Variation of the open circuit potential (OCP) of the iron in the acidic medium without and with different concentration of the Galactomannan.

The results show that the efficacy of inhibition decreases with increased concentration of inhibitors in the corrosive solution. It reached a maximum value of 87.72% at 1 g/l of the inhibitor. Hence, this research shows a good protective effect of galactomannan against iron corrosion in an acidic environment.

3.3.2. *Electrochemical measurements*

3.3.2.1. OCP. The curves of the OCP as a function of time of iron immersed in an acidic medium (HCl 1M) in the absence and presence of the Galactomannan are presented in Figure 3.

The variation of the OCP indicates that the steady state of the electrochemical system establishes at -480 mV/SCE in case of the blank and at -510 mV/SCE in the presence of 1 g/l of the galactomannan after 15 min.

The alterations of these OCP values in the presence of the inhibitor can be justified by the adsorption of the molecules of the inhibitor on the electrode surface. The EIS and potentiodynamic polarization measurements were realized after the steady state of the OCP.

3.3.2.2. Anodic and cathodic polarization curves (LP). Upon 30 min of immersion in 1 M HCl solution, the cathodic and anodic polarization curves were performed with and without varying concentrations of inhibitor. The curves of cathodic and anodic polarization are shown in Figure 4.

In the case of the blank, the corrosion potential is -471.20 mV/SCE. This potential shift toward more negative values in presence of the galactomannan with a decrease in the cathodic current densities following the Tafel variation region due to the reduction of H^+. The cathodic reaction was schematic by the following equation:

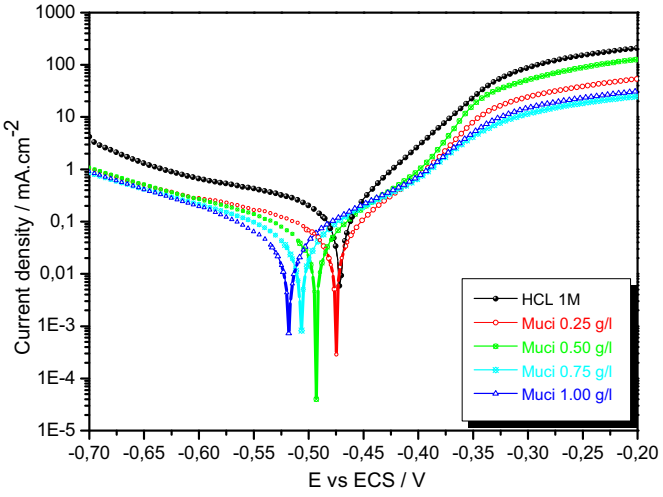

Figure 4. The anodic and cathodic plots of the iron electrode in the 1M HCl solution with and without the various concentration of the Galactomannan.

In the anodic branch, four potential zones are observed, the first zone is next to the corrosion potential E_{corr} = -471.2 mV/SCE as an exponential variation. The second zone is located between the potentials -480 mV/SCE and -380 mV/SCE, it is a pseudo-passivation plateau present. Afterwards a trans-passivation zone has appeared in a potential range between -380 and -300 mV/SCE. Finally, the film remains stable especially for a concentration of 1 g/l.

The following reaction corresponding to the anodic dissolution of the metal:

Table 3. The electrochemical parameters of the polarization curves of an iron electrode in a 1M HCl solution without and with different concentration of the Galactomannan.

Concentrations (g/l)	$-E_{corr}$ (mV/SCE)	i_{corr} (mA/cm^2)	-βc (mV/dec)	βa (mV/dec)	E (%)
Blank	471.20 ± 0.1	0.242 ± 0.001	269.7 ± 0.5	69.7 ± 0.6	–
0.25	474.68 ± 0.2	0.052 ± 0.002	228.5 ± 0.6	73.3 ± 0.4	78.3 ± 0.2
0.50	493.01 ± 0.2	0.049 ± 0.001	152.4 ± 0.4	66.8 ± 0.5	79.6 ± 0.2
0.75	505.83 ± 0.1	0.043 ± 0.002	150.7 ± 0.4	83.3 ± 0.6	82.1 ± 0.2
1.00	517.94 ± 0.1	0.032 ± 0.001	114.2 ± 0.3	77.3 ± 0.2	86.6 ± 0.2

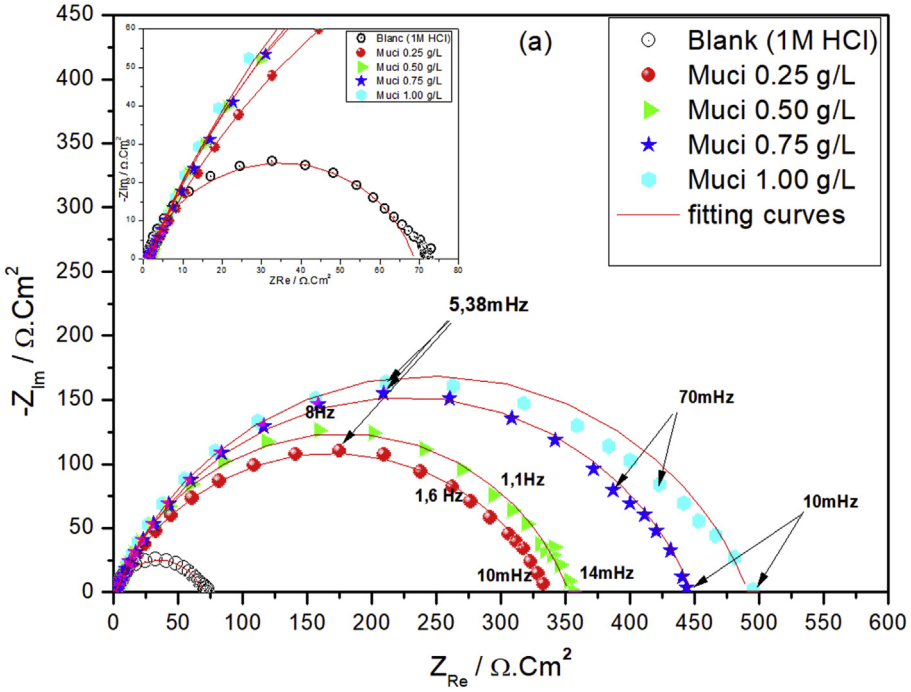

Figure 5. Nyquist diagrams of iron immersed in 1M HCl solution without and with different concentrations of the Galactomannan.

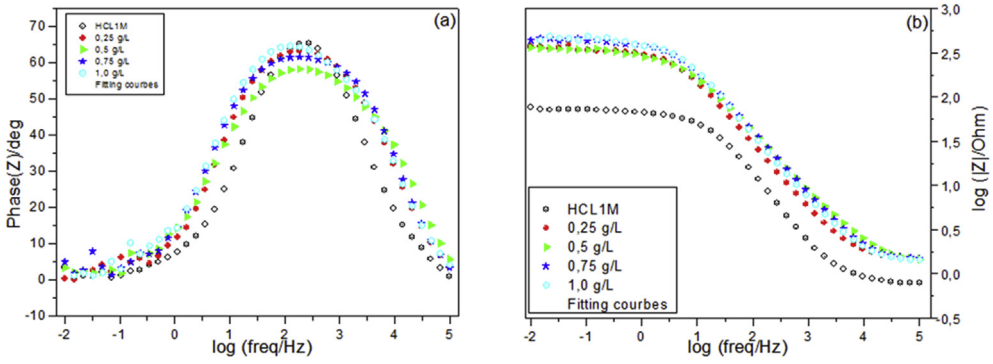

Figure 6. Bode diagrams of iron immersed in 1M HCl solution without and with different concentrations of the Galactomannan, (a) phase versus Log (Freq), (b) Module lZl versus Log (Freq).

The electrochemical parameters of the polarization curves are reported in the Table 3:

The current density values indicate that the oxidative dissolution of the electrode in the anodic section and the hydrogen reduction in the cathodic section were both weaker in the presence of the inhibitor. We also note that the inhibition efficiency increase with the increasing of the inhibitor concentration and this value reached 86.6% for a concentration of 1 g/l. This is due to the inhibitory film adsorption, which is reinforced by corrosion products on the metal surface and give it resistance against dissolution. In addition, the Cl^- ions has an important role in adsorption between the positive charge of inhibitor and the metallic surface charged positively.

3.3.2.3. Electrochemical impedance spectroscopy (EIS). The electrochemical impedance diagrams with and without of different concentrations of the inhibitor intended to complete the understanding of the corrosion and inhibition mechanisms [24, 26, 27, 28, 29] of iron in HCl 1M solution.

The Nyquist and Bode diagrams of iron immersed in 1M HCl solution with and without inhibitor concentrations after 30 min of immersion are presented in the following figures (Figures 5 and 6).

Figure 5, shows that the capacitive loop's diameter increase proportional with the concentrations of the inhibitor. This type of diagram generally indicates the charge transfer process controls the corrosion reaction. In fact, the Bode diagram detects only one time constant (Figure 6), and the same behavior is observed for all concentrations.

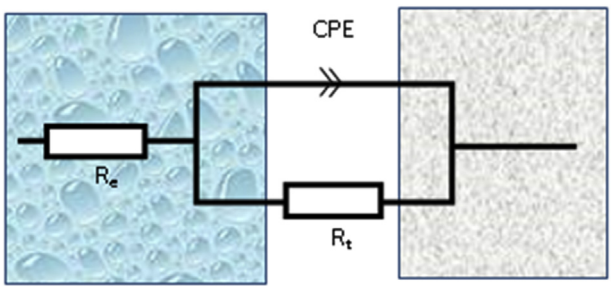

Figure 7. Equivalent electrical circuit of iron immersed in 1M HCl solution without and with different concentrations of the Galactomannan.

Table 4. The electrochemical parameters derived from Nyquist diagrams of an iron electrode in a 1M HCl solution without and with different concentration of the Galactomannan.

Concentrations (g/l)	R_e ($\Omega.cm^2$)	R_t ($\Omega.cm^2$)	CPE ($mF.n^{-1}$)	α	C_{dl} (mF)	E (%)
Blank	0.5 ± 0.1	68.5 ± 0.2	0.368 ± 0.002	0.70 ± 0.02	152.5 ± 0.2	–
0.25	1.3 ± 0.1	341.7 ± 0.2	0.245 ± 0.003	0.71 ± 0.02	0.917 ± 0.003	80 ± 0.1
0.50	1.3 ± 0.1	360.1 ± 0.2	0.210 ± 0.0015	0.73 ± 0.01	0.802 ± 0.001	81 ± 0.2
0.75	1.4 ± 0.1	446.6 ± 0.1	0.141 ± 0.004	0.79 ± 0.02	0.672 ± 0.004	84 ± 0.1
1.00	1.4 ± 0.1	490.4 ± 0.2	0.131 ± 0.005	0.78 ± 0.01	0.625 ± 0.005	86 ± 0.2

The modeling of these diagrams by the EC-Lab software led us to propose the following equivalent electrical circuit (Figure 7).

According to the electrochemical parameters determined by the equivalent circuit is summarized in the following table (Table 4).

Based on the obtained results, the resistance of the metal is higher in the presence of 1 g/l of the inhibitor (490.4 Ω) than in the case of the blank (68.5 Ω), which indicate a best inhibition behavior. The efficiency has reached a value of 86 % for concentration of the 1 g/l.

3.4. Immersion time effect

The evolution of electrochemical impedance spectroscopy diagrams at different immersion times of the iron electrode in a 1M HCl acidic medium in the presence of biopolymer at 1 g/l is displayed in Figure 8:

The obtained result shows that the electrochemical impedance diagrams maintain the same shape observed in the effect of the concentration study at the different immersion time. We note an increase in the size of the loop with the increase of immersion time. This is explained by the reinforcement of the barrier layer formed on the metal surface over time.

3.5. Adsorption isotherm

To know more about adsorption of the inhibitor molecules several types of isotherms adsorption were tested: Langmuir, Temkin, and Frumkin.

The isotherms adsorptions are described by the following equations:

- $\frac{C_{inh}}{\theta} = \frac{1}{K_{ads}} + C_{inh}$ Langmuir adsorption
- $\left(\frac{\theta}{1-\theta}\right)e^{-2a\theta} = K_{ads}C_{inh}$ FrumKin adsorption
- $e^{-2a\theta} = K_{ads}C_{inh}$ Temkin adsorption

Figure 9 shows the adsorption isotherms plotted at 298 K from the values obtained with the LP curves and EIS diagrams.

The parameters of the adsorption isotherm are determined by the following equation $\Delta G^0_{ads} = -RTLn(55.5.K)$ and reported in Table 5.

The negative values of G suggest spontaneous adsorption on an electrode surface of inhibitor molecules and good interaction between inhibitor molecules and the metal surface [30, 31, 32]. Generally, the $\mathbf{\Delta G^o_{ads}}$ value of -20 kJ/mol or less indicates an electrostatic interactions, this process is named physisorption; those that are more negative than -40 kJ/mol involve the sharing or electron transfer from the inhibitor molecules to the metallic surface to form a type of coordinated bond (chemisorption) [33, 34]. The ΔG^o_{ads} values obtained for biopolymer (-24.26 kJ/mol for LP and -25.11 kJ/mol for SIE) likely mean that the metal surface adsorption process could be due to physisorption and chemisorption at the same time as the electrostatic interactions predominate [35, 36]. It is a complex phenomenon of interactions. Indeed, according to the literature [37, 38], It should also be noted that the high K_{ads} values refer to high adsorption might indicate that biopolymer is a good inhibitory effect.

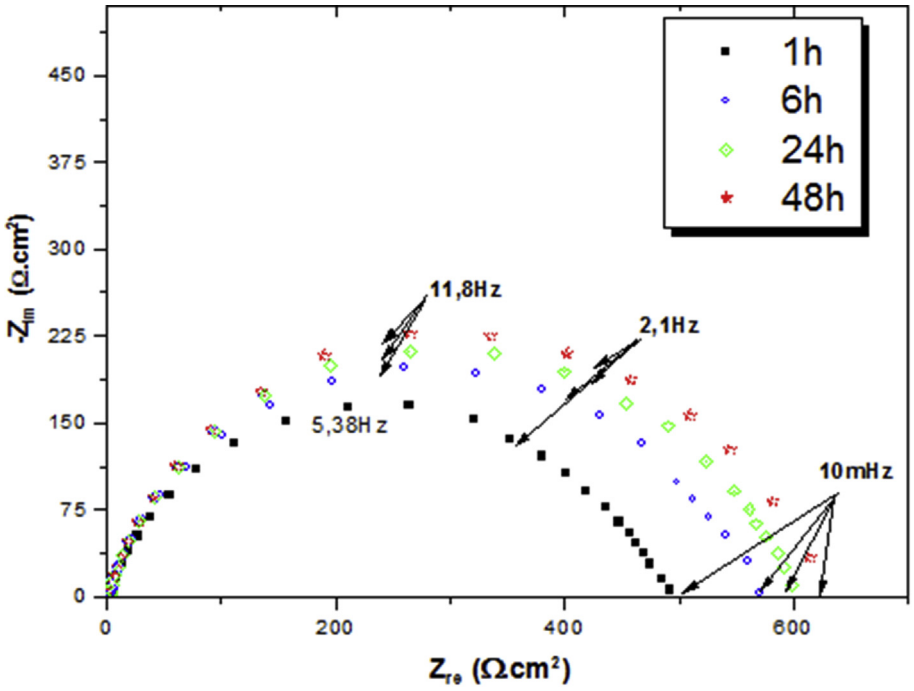

Figure 8. Electrochemical impedance diagrams at different immersion times of an iron electrode in a 1M HCl solution in presence of the inhibitor (1 g/l).

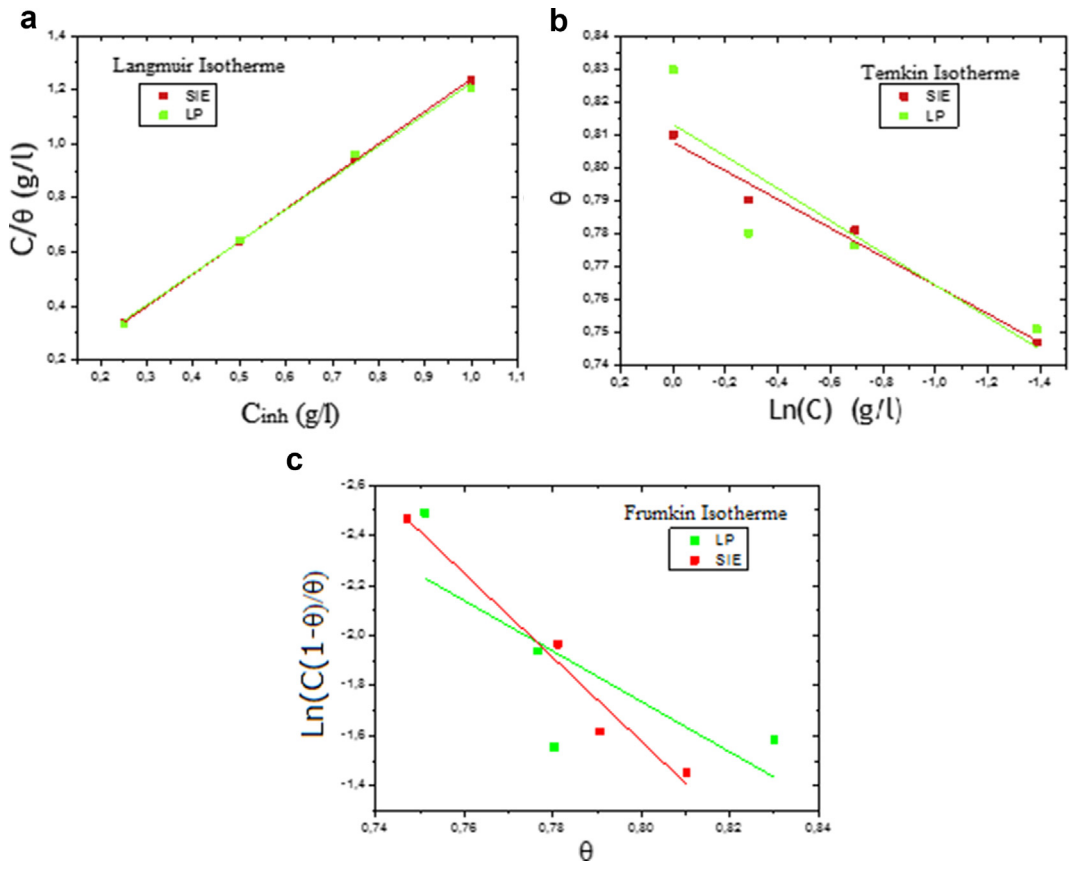

Figure 9. Adsorption isotherms obtained for iron in 1 M HCl solution in the presence of 1 g/L of the GalaThe analysis of these adsorption isotherms shows that the ratio C_{inh}/θ variation (isotherm Langmuir) as a function of inhibitor concentration is linear. This behavior indicates that the adsorption of inhibitor molecules on the iron surface in the HCl 1 *M media* approaches the adsorption isotherm of the Langmuir. Hence, inhibition of corrosion is due to the formation of a monolayer on the electrode surface, which limits access to electrolytes.

3.6. UV-visible analysis

The aim of UV-visible analysis is to identify the interaction surface metallic-inhibitor molecules. Figure 10 presents the UV-Visible spectrum of the solution before and after immersion in solution (1M HCl+1 g/l of the inhibitor).

It would seen from the spectra those two peaks, the first between 200 nm and 280nm attributed to π-π* transition and the second between 280 nm and 400 nm attributed σ–π transitions of the oxygen atoms [39]. It is noted that the spectrum after immersion, the adsorption peak 310 nm move to 328 nm. This bathochromic shift suggests a formation of the inhibitor-metal complex in acidic solution by transfer of the charges between the sites of the inhibitor molecules having a high electron density and vacuum d orbital of iron. As a result, UV-visible spectra confirm the adsorption capacity of the polysaccharide on the surface of iron and thereby a formation of Fe–inhibitor complex film on the surface metallic [40, 41].

3.7. Surface analysis

The surface analysis was performed using the SEM technique coupled with the EDS elemental analysis to estimate the morphology of the surface of the iron substrate in 1M HCl solution.

Table 5. Langmuir adsorption isotherm parameters.

Test	$-\Delta G^{o}_{ads}$(Kcal.mol^{-1})	K_{ads} (M^{-1})	R^2	Slope
LP	24.26	17.86	0.99	1.1167
SIE	25.11	25.19	0.99	1.1306

The SEM micrographs and EDS spectra corresponding to the iron substrate after 24 h of immersion in 1M HCl solution, in the absence and in the presence of a concentration of 1 g/l of biopolymer are shown in Figure 11 (a, b, c) respectively.

From Figure (11b), it is noted that the SEM micrograph revealed in the absence of the inhibitor a severe attack by aggressive solution compared to the SEM micrographs in Figure (11a, c) on the surface of the iron studied. The EDS spectrum shows characteristic peaks of the iron substrate and a high presence of oxygen atoms (oxide of iron). In

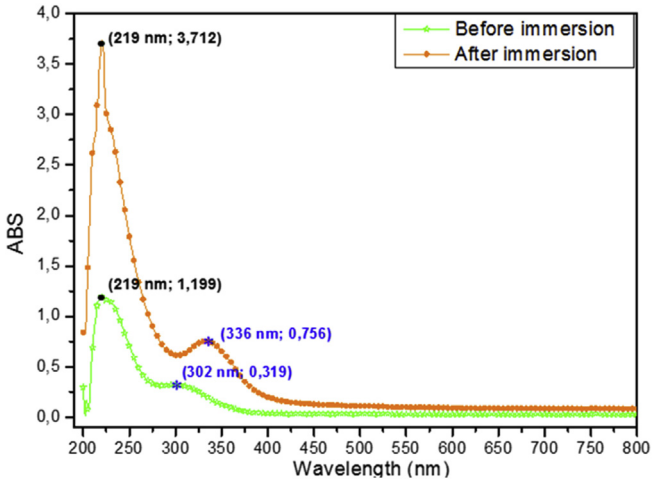

Figure 10. UV-visible spectrum for solution (1 M HCl +1 g/l inhibitor) before and after 48h of immersion of iron substrate.

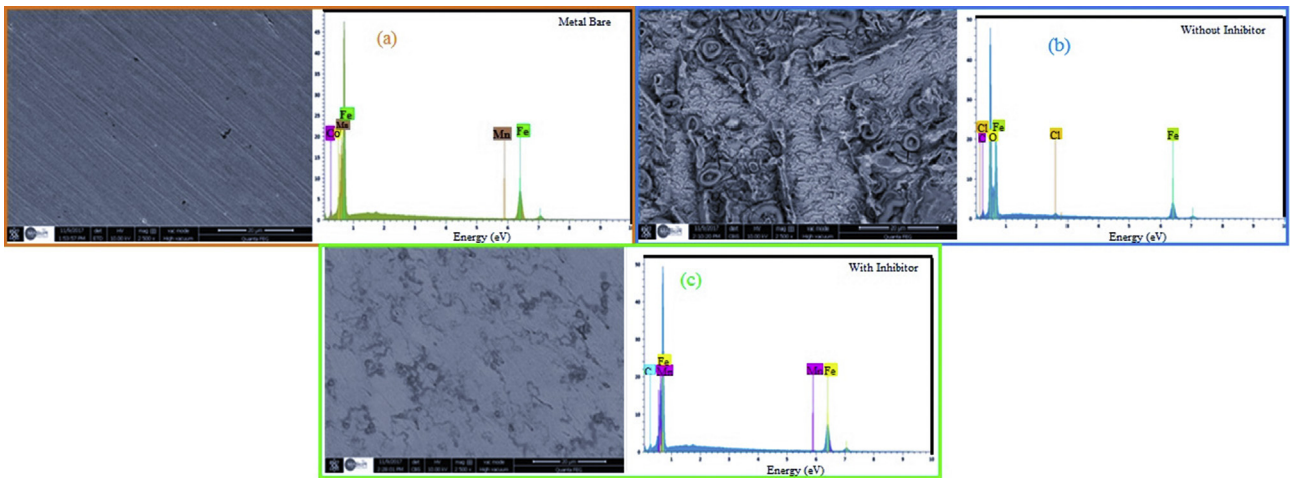

Figure 11. SEM micrograph and EDS spectrum of the iron substrate: (a): The iron surface. (b): The iron surface in case of the blank (HCl 1M). (c): The iron surface in solution with inhibitor.

addition, a completely different situation was detected in the presence of the inhibitor.

The visualization of the SEM micrograph from Figure (11c) shows that the metal surface remains intact. In addition, the metal surface of the electrode is smooth. This may be related to the establishment of the inhibitor film on the metal surface. This is confirmed by the analysis of the EDS spectrum, which signals a less intense oxygen peak.

These results confirm the high inhibition efficiency values obtained by electrochemical and gravimetric measurements that can be attributed to the effective protection of the galactomannan as inhibitor by the formation of an inhibitor film on the surface of the iron substrate.

3.8. Theoretical calculations

3.8.1. DFT result

Theoretical parameters were performed using the functional density theory method. The distribution of the HOMO and the LUMO orbital is a critical tool to predict the capacity adsorption of the inhibitor molecules.

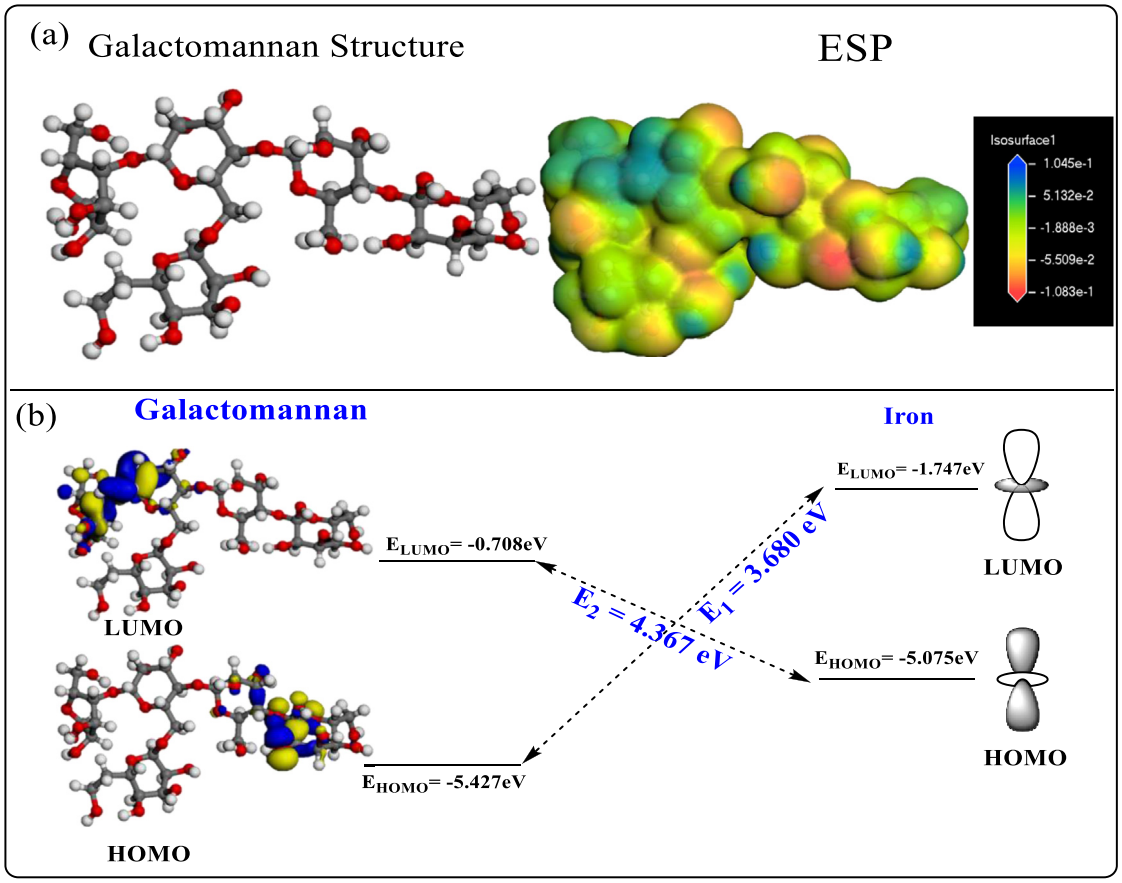

Figure 12. (a) distribution of the frontiers orbitals (HOMO and LUMO) of the inhibitor and ESP and (b) Schematic illustration of the Iron-Galactomannan interactions.

The ability of molecule to share their electron with others orbital vacant is indicated by high energy (E_{HOMO}) and the low energy (E_{LUMO}).

From the distribution of the inhibitor's HOMO and LUMO frontier orbital (Figure 12), it is clear that the distribution of HOMO and LUMO density is located on the oxygen atoms, these sites are responsible for giving electrons to the metal surface [42]. The differences between E_{LUMO} of Galactomannan and E_{HOMO} of iron (E2) and vice versa (E1) were therefore determined and shown in Figure 12. Analysis of Figure 12 revealed that E_2 was greater than E_1, indicating that Galactomannan is better an electron donor than an electron receptor. Therefore, the ability to inhibit corrosion of Galactomannan could be compared on the basis of the electron donation capability. Both the facts suggested that the Galactomannan would primarily control the inhibition capability. The bonds between the Galactomannan and the Iron could be formed by sharing the electrons donated by the Galactomannan; however, The Galactomannan will play a key role in that. Bond formation is also possible through back donation (iron-donated electron), especially in Galactomannan as E_1 is closely related to E_2. Overall, the preliminary examination of the Galactomannan by DFT calculations has proposed that Galactomannan could act as corrosion inhibitor for mild steel.

The ionization energy and electron affinity were determined by the following equations:

$$I = -E_{HOMO}$$

$$A = -E_{LUMO}$$

The obtained results (Table 6) indicate that the ionization energy reached a value of 5.427 eV, therefore; the electron affinity attended a value of 0.708 eV. In addition, the value of the gap energy (ΔEgap) equal 4.719 eV, it is the lowest value, which can explain the good protective property of the inhibitor. Indeed, the value of charge transfer ΔN which indicates the ability of a molecule to share its electrons with the metal is ΔN = 0.833. This value suggests the highest capacity of the molecular matrix to donate electrons to the metallic surface.

3.8.2. Distribution of the Mulliken atomic charge and dipole moment

The Mulliken atomic charge distribution presents the nucleophilic and electrophilic attack sites. The Figure 13 shows the direction of the dipole moment and the Mulliken atomic charges of the biopolymer atoms.

Based on this result, we conclude that the nucleophilic and electrophilic sites were the carbon and oxygen atoms [36].

3.8.3. Simulation by MD

In order to determine the best adsorption configuration, the optimization of the adsorption of molecule inhibitor was performed. The result of this calculation was presented in Figure 14.

From the figure, the optimum energy has reached less than -3241.32 Ha.

To study the energy fluctuation interactions between the inhibitor molecule, the metallic surface and the water molecules were calculated using simulation by MD to optimize the entire Fe_{110}/inhibitor/H_2O system.

The distribution of the adsorption energy for "Fe_{110}/inhibitor/H_2O" in the solution of the hydrochloric acid by the model of the adsorption localization is given in Figure 15.

The inhibitor molecules energy is equal to -256000 cal/mol, this signifies an important tolerance of the adsorption capacity on the metallic area [43].

Table 6. Quantum parameters of the inhibitor.

Quantum parameters	E_{HOMO} (eV)	E_{LUMO} (eV)	ΔE_{gap} (eV)	ΔN
Values	-5.427	-0.708	4.719	0.833

The Figure 16 presents the distance between the inhibitor molecule and the electrode surface.

According to the RDF calculation result, the first peak at 2.5 Å indicates chemisorption interactions and for the peaks above 3.5 Å are associated to the physical interactions, that explain the capacity of the biopolymer to stop the dissolution of metal by the ability of the biopolymer molecules to give his electrons to the metal and vice versa. This result conformed to the isotherm adsorption result [41, 42].

3.8.4. MD result

The lateral and Up views of the most stable low energy for the best adsorption configuration of the inhibitory molecule adsorption are presented in the Figure 17.

Examination of the Figure 17, indicate that the biopolymer flatly adsorbed on the metallic surface and covered a large area of the electrode [44,45]. The parameters are given in Table 7.

In addition, the basic superposition error (BSSE) was used to correct the E_{ads} on the metallic of the Fe_{110} with the water molecule. The energy for adsorption is provided by formula 3 [46].

$$E_{Ads} = E_{\left(\frac{Fe_{110}}{\text{Galactomannan}/H_2O}\right)} - \left(E_{\text{Galactomannan}} - E_{Fe_{110}} - E_{H_2O}\right) \quad (3)$$

Adsorption energy is defined as the algebraic addition of rigid adsorption energy (R.A.E.) and deformation energy (DE) for adsorbed components. The rigid adsorption energy, therefore, reports the released energy (Kcal/mol) when the unreleased adsorbate macromolecular matrix is released, before the geometry optimization step that is adsorbed on the iron surface (Fe_{110}) in the presence of 900 water molecules. While the deformation energy (DE) reports the energy released (Kcal/mol) when adsorbed molecules of the Galactomannan is released on the Fe surface (Fe_{110}). Table 7 also gives the desorption energy (dE_{ads}/dN_i) which reports the energy of the substrate-adsorbate configuration where one of the adsorbed components has been removed [47].

From Table 7, it is clear that the values of the adsorption energies are negative, which means that adsorption of the inhibitor studied could occur spontaneously [48]. The high adsorption energy (-12300 $Kcal.mol^{-1}$) of the inhibitor molecule indicates that the adsorption of the inhibitory macromolecular matrix on the Fe surface (Fe_{110}) is adsorbed by involving the displacement of the H_2O molecules on the iron surface and sharing of electrons between the heteroatoms in the biopolymer inhibitor and the Fe surface (Fe_{110}). This gives the possibility of formation of coordination binding (vacant n-orbital) resulting from the overlapping of electrons (3d) of the iron atom and the free doublet of oxygen atoms.

The high values of the inhibitor's adsorption energies are due to parallel adsorption and the existence of a pair of electrons on the heteroatoms, promoting greater adsorption on the Fe surface (Fe_{110}). Metal surface protection is done by strong adsorption of the molecular and by preventing it from being freely rusted [49].

4. Conclusion

In this work, the galactomannan extracted from carob seeds and characterized by elemental analysis and FTIR analysis. The corrosion inhibition effect of biopolymer against iron corrosion in 1M HCl medium was studied by electrochemical methods and theoretical study (DFT and Molecular Dynamics) conformed that:

- Inhibition efficiency improves with increasing inhibitor concentrations and achieves a highest value of 87.7% for a concentration of 1g/l in biopolymer. In addition to acting as a mixed inhibitor with a mainly cathodic character, the immersion time test also shows that the protective effect of biopolymer increases with increased immersion time.

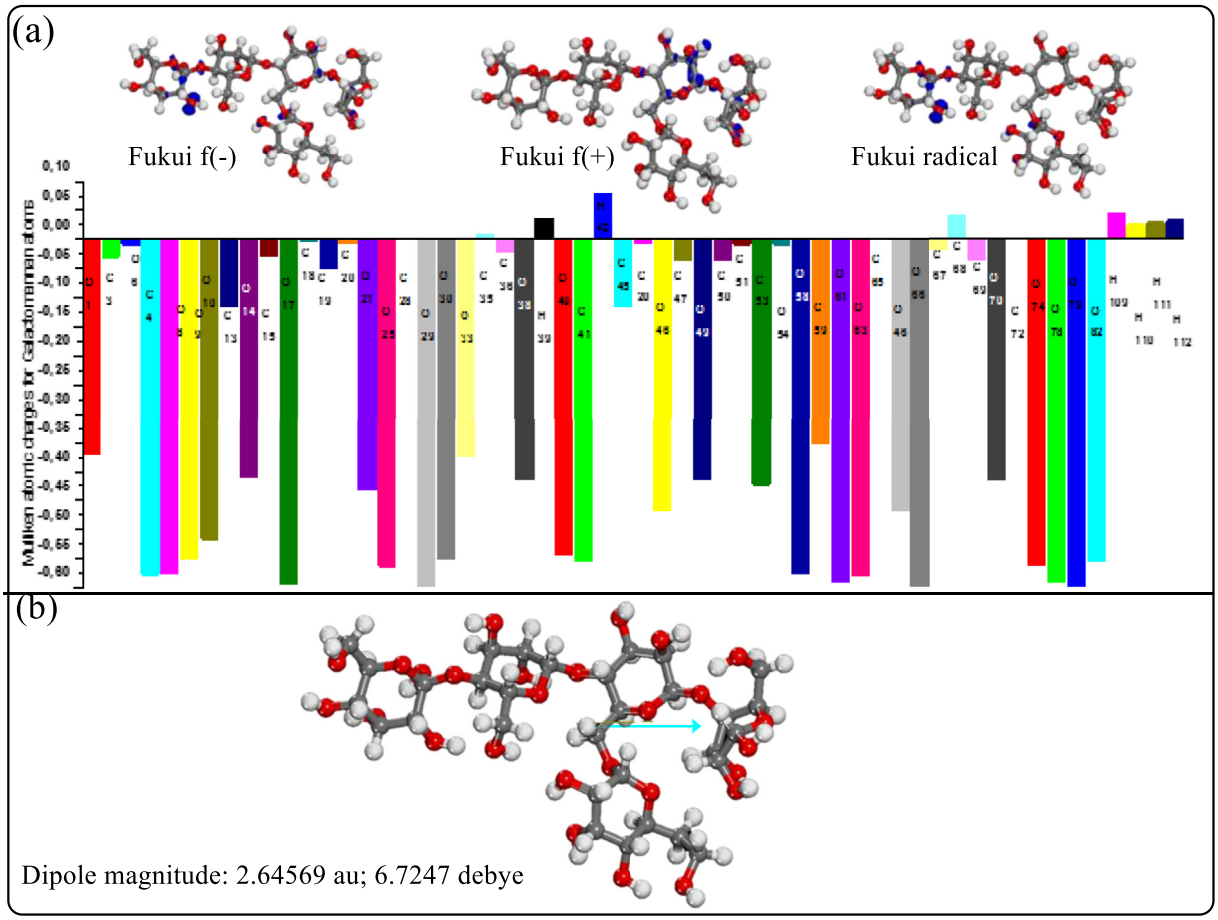

Figure 13. (a): Milliken atomic charges for the Galactomannan atoms (b): Direction of the dipole moment.

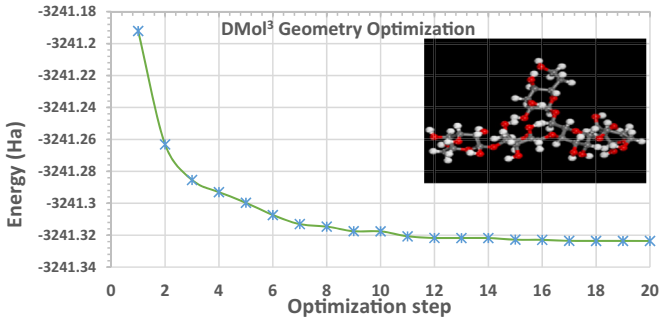

Figure 14. Optimization energy of biopolymer in neutral forms.

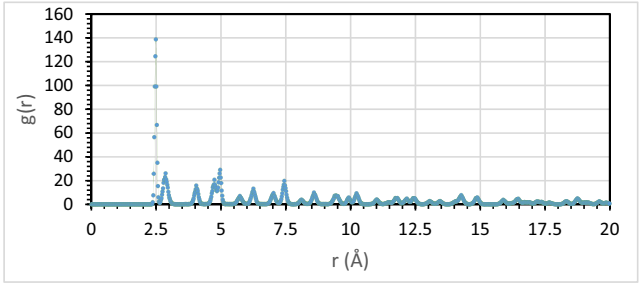

Figure 16. Radial distribution of molecule on the surface Fe_{110} in solution.

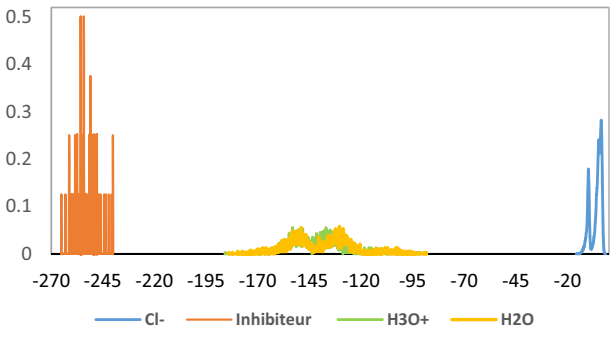

Figure 15. Distribution of adsorption energy of the Fe_{110}/inhibitor/H2O system.

- The adsorption of biopolymer compounds on the iron surface assumes the isotherm of Langmuir.
- Surface analysis using SEM/EDS confirms the high inhibition efficiency values that can be attributed to the effective protection of the inhibitor by the formation of an inhibitor film on the iron surface.
- UV-Vis spectroscopy measurements approve the complexation capacity of the biopolymer with metal surface.
- Theoretical calculations imply that oxygen atoms may serve as adsorption sites linking the molecule and the iron. Molecular simulation reveals that the biopolymer can be adsorbed on the iron surface in a closely paralleled way with O–Fe bonds by physisorption and chemisorption at the same time with a high proportion of electrostatic interaction that confirms the result obtained in the isotherm adsorption studies and experimental techniques.

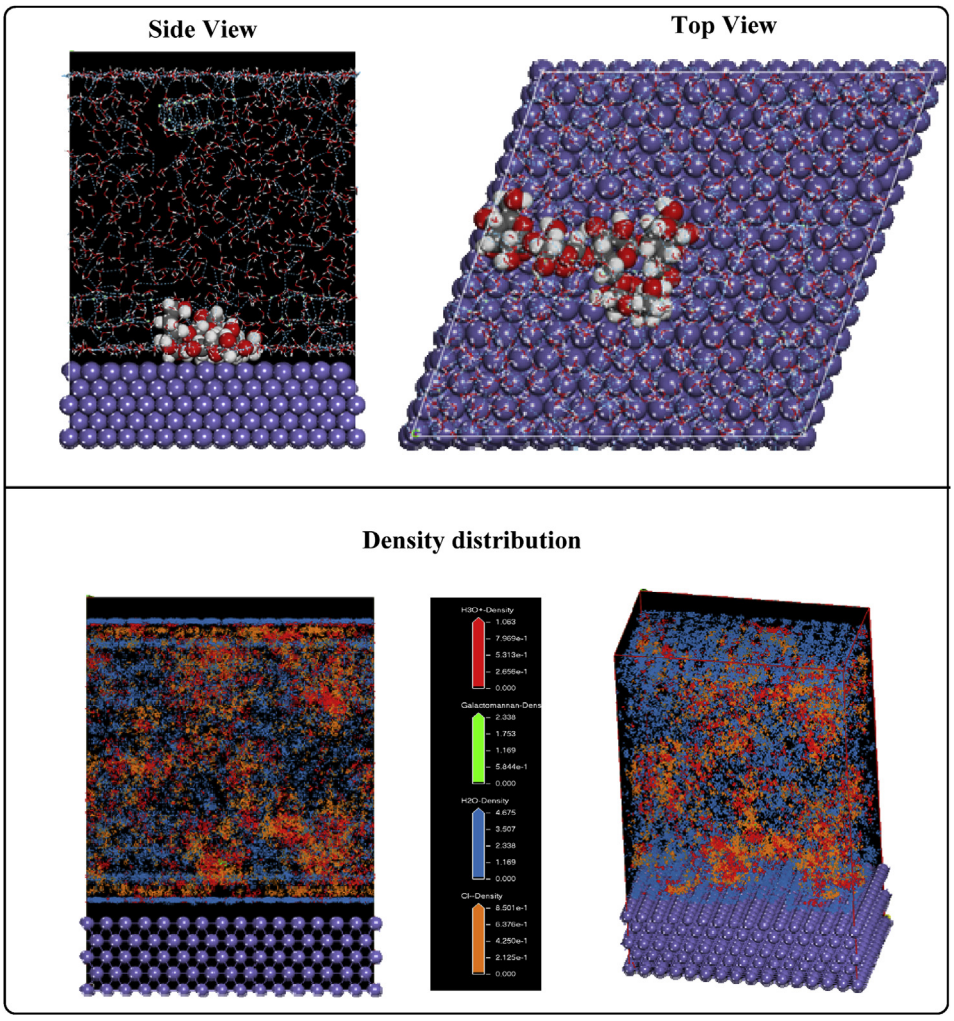

Figure 17. Lateral and Up views of the adsorption (Fe_{110}/Biopolymer/H_2O) and density distribution.

Table 7. Module results of the adsorption location for the two lowest adsorption configurations for the Fe_{110}/biopolymer/H_2O system (all values are expressed in Kcal.mol^{-1}).

Structures	Total energy	Adsorption energy	Rigid adsorption energy	Deformation energy	H_2O dE_{ads}/dNi	Biopolymer dE_{ads}/dNi	H_3O^+ dE_{ads}/dNi	Cl^-dE_{ads}/dNi
Fe $_{(1\ 1\ 0)}$- 1	-1.10E+04	-1.23E+04	-1.10E+04	-1.27E+03	-2.63557655	-257.4564402	-116.2745507	-97.73692956
Fe $_{(1\ 1\ 0)}$- 2	-1.10E+04	-1.23E+04	-1.10E+04	-1.27E+03	-2.32852099	-257.5146105	-111.9941413	-101.2981867
Fe $_{(1\ 1\ 0)}$- 3	-1.10E+04	-1.23E+04	-1.10E+04	-1.27E+03	-2.38070454	-257.5646012	-108.1556461	-98.07148263
Fe $_{(1\ 1\ 0)}$- 4	-1.09E+04	-1.22E+04	-1.10E+04	-1.27E+03	-2.65901238	-253.2580086	-119.431887	-94.93615438
Fe $_{(1\ 1\ 0)}$- 5	-1.09E+04	-1.22E+04	-1.09E+04	-1.27E+03	-2.56776181	-246.2822784	-112.6300862	-121.9286112
Fe $_{(1\ 1\ 0)}$- 6	-1.09E+04	-1.22E+04	-1.09E+04	-1.27E+03	-2.64790532	-263.1975541	-114.8186211	-123.0942572
Fe $_{(1\ 1\ 0)}$- 7	-1.09E+04	-1.22E+04	-1.09E+04	-1.27E+03	-2.67669919	-243.4711702	-107.4778163	-118.3733126
Fe $_{(1\ 1\ 0)}$- 8	-1.09E+04	-1.22E+04	-1.09E+04	-1.27E+03	-2.37155126	-247.9988459	-110.1802914	-112.4768141
Fe $_{(1\ 1\ 0)}$- 9	-1.09E+04	-1.22E+04	-1.09E+04	-1.27E+03	-2.55320196	-240.1172149	-109.4516229	-121.8911257
Fe $_{(1\ 1\ 0)}$- 10	-1.09E+04	-1.22E+04	-1.09E+04	-1.27E+03	-2.40380421	-258.4377035	-113.7561265	-101.4365418

Declarations

Author contribution statement

Said ABBOUT: Conceived and designed the experiments; Performed the experiments; Analyzed and interpreted the data; Contributed reagents, materials, analysis tools or data; Wrote the paper.

Meryem ZOUARHI: Conceived and designed the experiments.

Driss CHEBABE: Analyzed and interpreted the data.

Mohamed DAMEJ, Avni BERISHA: Contributed reagents, materials, analysis tools or data.

Najat HAJJAJI: Analyzed and interpreted the data.

Funding statement

This research did not receive any specific grant from funding agencies in the public, commercial, or not-for-profit sectors.

Competing interest statement

The authors declare no conflict of interest.

Additional information

No additional information is available for this paper.

References

[1] M.S. Al-Otaibi, A.M. Al-Mayouf, M. Khan, A.A. Mousa, S.A. Al-Mazroa, H.Z. Alkhathlan, Corrosion inhibitory action of some plant extracts on the corrosion of mild steel in acidic media, Arabian J. Chem. 7 (2014) 340–346.

[2] M. Zouarhi, M. Chellouli, S. Abbout, H. Hammouch, A. Dermaj, S.O. Said Hassane, P. Decaro, N. Bettach, N. Hajjaji, A. Srhiri, Inhibiting effect of a green corrosion inhibitor containing Jatropha Curcas seeds oil for iron in an acidic medium, Port. Electrochim. Acta 36 (2018) 179–195.

[3] M. Chellouli, D. Chebabe, A. Dermaj, H. Erramli, N. Bettach, N. Hajjaji, M.P. Casaletto, C. Cirrincione, A. Privitera, A. Srhiri, Corrosion inhibition of iron in acidic solution by a green formulation derived from Nigella sativa L, Electrochim. Acta 204 (2016) 50–59.

[4] S. Abbout, M. Chellouli, M. Zouarhi, B. Benzidia, H. Hammouch, D. Chebabe, A. Dermaj, H. Erramli, N. Bettach, N. Hajjaji, New formulation based on Ceratonia siliqua L seed oil, as a green corrosion inhibitor of iron in acidic medium, Anal. Bioanal. Electrochem. 10 (2018) 789–804.

[5] M. Abdallah, Guar gum as corrosion inhibitor for carbon steel in sulfuric acid solutions, Port. Electrochim. Acta 22 (2004) 161–175.

[6] S.A. Umoren, U.M. Eduok, Application of carbohydrate polymers as corrosion inhibitors for metal substrates in different media: a review, Carbohydr. Polym. 140 (2016) 314–341.

[7] A. Jano, A. Lame, E. Kokalari, Use of extracted green inhibitors as a friendly choice in corrosion protection of low alloy carbon steel, Kem Ind. 61 (2012) 497–503.

[8] R. Brown, R. Mears, The electrochemistry of corrosion, Trans. Electrochem. Soc. 74 (1938) 495–517.

[9] S. Marzorati, L. Verotta, S. Trasatti, Green corrosion inhibitors from natural sources and biomass wastes, Molecules 24 (2019) 48.

[10] P.A. Dakia, B. Wathelet, M. Paquot, Isolation and chemical evaluation of carob (Ceratonia siliqua L.) seed germ, Food Chem. 102 (2007) 1368–1374.

[11] P.A. Dakia, C. Blecker, C. Robert, B. Wathelet, M. Paquot, Composition and physicochemical properties of locust bean gum extracted from whole seeds by acid or water dehulling pre-treatment, Food Hydrocolloids 22 (2008) 807–818.

[12] M.S. Kök, A comparative study on the compositions of crude and refined locust bean gum: in relation to rheological properties, Carbohydr. Polym. 70 (2007) 68–76.

[13] S. Kumazawa, M. Taniguchi, Y. Suzuki, M. Shimura, M.-S. Kwon, T. Nakayama, Antioxidant activity of polyphenols in carob pods, J. Agric. Food Chem. 50 (2002) 373–377.

[14] N. Bouzouita, A. Khaldi, S. Zgoulli, L. Chebil, R. Chekki, M.M. Chaabouni, P. Thonart, The analysis of crude and purified locust bean gum: a comparison of samples from different carob tree populations in Tunisia, Food Chem. 101 (2007) 1508–1515.

[15] R.O. Mannion, C.D. Melia, B. Launay, G. Cuvelier, S.E. Hill, S.E. Harding, J.R. Mitchell, Xanthan/locust bean gum interactions at room temperature, Carbohydr. Polym. 19 (1992) 91–97.

[16] B.A. Boukamp, Equivalent Circuit, Princeton Applied Research Corporation, Princeton, NJ, 1990.

[17] K. Rahmouni, S. Joiret, L. Robbiola, A. Srhiri, H. Takenouti, V. Vivier, Corrosion and protection of B3 bronze covered with patina in NaHCO 3+ Na 2 SO 4 solution simulating an acid rain in urban environment, Impedance Commun. On Line 2 (2004).

[18] M.A. Amin, Weight loss, polarization, electrochemical impedance spectroscopy, SEM and EDX studies of the corrosion inhibition of copper in aerated NaCl solutions, J. Appl. Electrochem. 36 (2006) 215–226.

[19] M.J. Frisch, G.W. Trucks, H.B. Schlegel, G.E. Scuseria, M.A. Robb, J.R. Cheeseman, J.A. Montgomery Jr., T. Vreven, K.N. Kudin, J.C. Burant, J.M. Millam, S.S. Iyengar, J. Tomasi, V. Barone, B. Mennucci, M. Cossi, G. Scalmani, N. Rega, G.A. Petersson, H. Nakatsuji, M. Hada, M. Ehara, K. Toyota, R. Fukuda, J. Hasegawa, M. Ishida, T. Nakajima, Y. Honda, O. Kitao, H. Nakai, M. Klene, X. Li, J.E. Knox, H.P. Hratchian, J.B. Cross, C. Adamo, J. Jaramillo, R. Gomperts, R.E. Stratmann, O. Yazyev, A.J. Austin, R. Cammi, C. Pomelli, J.W. Ochterski, P.Y. Ayala, K. Morokuma, G.A. Voth, P. Salvador, J.J. Dannenberg, V.G. Zakrzewski, S. Dapprich, A.D. Daniels, M.C. Strain, O. Farkas, D.K. Malick, A.D. Rabuck, K. Raghavachari, J.B. Foresman, J.V. Ortiz, Q. Cui, A.G. Baboul, S. Clifford, J. Cioslowski, B.B. Stefanov, G. Liu, A. Liashenko, P. Piskorz, I. Komaromi, R.L. Martin, D.J. Fox, T. Keith, M.A. Al-Laham, C.Y. Peng, A. Nanayakkara, M. Challacombe, P.M.W. Gill, B. Johnson, W. Chen, M.W. Wong, C. Gonzalez, J.A. Pople, Gaussian, Inc., Wallingford CT, 2004.

[20] Z. Zhang, N.C. Tian, X.D. Huang, W. Shang, L. Wu, Synergistic inhibition of carbon steel corrosion in 0.5 M HCl solution by indigo carmine and some cationic organic compounds: experimental and theoretical studies, RSC Adv. 6 (2016) 22250–22268.

[21] L. Guo, C. Qi, X. Zheng, R. Zhang, X. Shen, S. Kaya, Toward understanding the adsorption mechanism of large size organic corrosion inhibitors on an Fe(110) surface using the DFTB method, RSC Adv. 7 (2017) 29042–29050.

[22] H. Neukom, Carob bean gum: properties and applications, in: P. Fito, A. Mulet (Eds.), Proceedings of the III International Carob Symposium. Valencia, Spain, 1988, pp. 551–555.

[23] A. Lazaridou, C.G. Biliaderis, M.S. Izydorczyk, Structural characteristics and rheological properties of locust bean galactomannans: a comparison of samples from different carob tree populations, J. Sci. Food Agric. 81 (2001) 68–75.

[24] D.A. Harrington, P. Van Den Driessche, Mechanism and equivalent circuits in electrochemical impedance spectroscopy, Electrochim. Acta 56 (2011) 8005–8013.

[25] R.C.M. De Paula, J.F. Rodrigues, Composition and rheological properties of cashew tree gum, the exudate polysaccharide from Anacardium occidentale L, Carbohydr. Polym. 26 (1995) 177–181.

[26] J.-H. Chang, J. Park, Y. Kim Pak, J. Jungho Pak, Fitting Improvement Using a New Electrical Circuit Model for the Electrode-Electrolyte Interface Proceedings of the 3rd International IEEE EMBS Conference on Neural Engineering Kohala Coast, 2007, p. 2. Hawaii, USA.

[27] A. Dermaj, D. Chebabe, N. Hajjaji, V. Vivier, Use of electrochemical measurements and surface analysis for the evaluation of the protective properties of 3-phenyl-1, 2, 4-tiazole-5-thione formulation of metallic cultural heritage, Research & Reviews on Electrochemistry 4 (2013) 147–154.

[28] D.A. Lopez, S.N. Simison, S.R. De Sanchez, The influence of steel microstructure on CO2 corrosion. EIS studies on the inhibition efficiency of benzimidazole, Electrochim. Acta 48 (2003) 845–854.

[29] A.A. Hermas, M.S. Morad, M.H. Wahdan, Effect of PgTPhPBr on the electrochemical and corrosion behaviour of 304 stainless steel in H 2 SO 4 solution, J. Appl. Electrochem. 34 (2004) 95–102.

[30] E. Bayol, A. Gurten, M. Dursun, K. Kayakirilmaz, Adsorption behavior and inhibition corrosion effect of sodium carboxymethyl cellulose on mild steel in acidic medium, Acta Phys. Chim. Sin. 24 (2008) 2236–2243.

[31] O.K. Abiola, N.C. Oforka, Adsorption of (4-amino-2-methyl-5-pyrimidinyl methylthio) acetic acid on mild steel from hydrochloric acid solution (HCl)—Part 1, Mater. Chem. Phys. 83 (2004) 315–322.

[32] A.A. Fadhil, A.A. Khadom, H. Liu, C. Fu, J. Wang, N.A. Fadhil, H.B. Mahood, (S)-6-Phenyl-2,3,5,6-tetrahydroimidazo[2,1-b] thiazole hydrochloride as corrosion inhibitor of steel in acidic solution: gravimetrical, electrochemical, surface morphology and theoretical simulation, J. Mol. Liq. 276 (2019) 503–518.

[33] F. Bentiss, M. Lebrini, M. Lagrenée, Thermodynamic characterization of metal dissolution and inhibitor adsorption processes in mild steel/2,5-bis(n-thienyl)-1,3,4-thiadiazoles/hydrochloric acid system, Corrosion Sci. 47 (2005) 2915–2931.

[34] T.J. Harvey, F.C. Walsh, A.H. Nahlé, A review of inhibitors for the corrosion of transition metals in aqueous acids, J. Mol. Liq. (2018).

[35] X. Li, S. Deng, H. Fu, X. Xie, Synergistic inhibition effects of bamboo leaf extract/major components and iodide ion on the corrosion of steel in H3PO4 solution, Corrosion Sci. 78 (2014) 29–42.

[36] K.R. Ansari, M.A. Quraishi, A. Singh, Schiff's base of pyridyl substituted triazoles as new and effective corrosion inhibitors for mild steel in hydrochloric acid solution, Corrosion Sci. 79 (2014) 5–15.

[37] I. Ahamad, R. Prasad, M.A. Quraishi, Thermodynamic, electrochemical and quantum chemical investigation of some Schiff bases as corrosion inhibitors for mild steel in hydrochloric acid solutions, Corrosion Sci. 52 (2010) 933–942.

[38] Y. Kharbach, F.Z. Qachchachi, A. Haoudi, M. Tourabi, A. Zarrouk, C. Jama, L.O. Olasunkanmi, E.E. Ebenso, F. Bentiss, Anticorrosion performance of three newly synthesized isatin derivatives on carbon steel in hydrochloric acid pickling environment: electrochemical, surface and theoretical studies, J. Mol. Liq. 246 (2017) 302–316.

[39] M. Rbaa, A.S. Abousalem, M.E. Touhami, I. Warad, F. Bentiss, B. Lakhrissi, A. Zarrouk, Novel Cu (II) and Zn (II) complexes of 8-hydroxyquinoline derivatives as effective corrosion inhibitors for mild steel in 1.0 M HCl solution: computer modeling supported experimental studies, J. Mol. Liq. 290 (2019) 111243.

[40] D.K. Yadav, M.A. Quraishi, Application of some condensed uracils as corrosion inhibitors for mild steel: gravimetric, electrochemical, surface morphological, UV–visible, and theoretical investigations, Ind. Eng. Chem. Res. 51 (2012) 14966–14979.

[41] M. Rbaa, F. Benhiba, I.B. Obot, H. Oudda, I. Warad, B. Lakhrissi, A. Zarrouk, Two new 8-hydroxyquinoline derivatives as an efficient corrosion inhibitors for mild steel in hydrochloric acid: synthesis, electrochemical, surface morphological, UV–visible and theoretical studies, J. Mol. Liq. 276 (2019) 120–133.

[42] M. Touil, N. Hajjaji, D. Sundholm, H. Rabaâ, Computational studies of the corrosion-inhibition efficiency of iron by triazole surfactants, Int. J. Quant. Chem. 113 (2013) 1365–1371.

[43] R. Hsissou, O. Dagdag, S. Abbout, F. Benhiba, M. Berradi, M. El Bouchti, A. Berisha, N. Hajjaji, A. Elharfi, Novel derivative epoxy resin TGETET as a corrosion inhibition of E24 carbon steel in 1.0 M HCl solution. Experimental and computational (DFT and MD simulations) methods, J. Mol. Liq. 284 (2019) 182–192.

[44] A. Singh, K.R. Ansari, Y. Lin, M.A. Quraishi, H. Lgaz, I.-M. Chung, Corrosion inhibition performance of imidazolidine derivatives for J55 pipeline steel in acidic oilfield formation water: electrochemical, surface and theoretical studies, J. Taiwan Inst. Chem. Eng. 95 (2019) 341–356.
[45] Q.H. Zhang, B.S. Hou, N. Xu, W. Xiong, H.F. Liu, G.A. Zhang, Effective inhibition on the corrosion of X65 carbon steel in the oilfield produced water by two Schiff bases, J. Mol. Liq. 285 (2019) 223–236.
[46] S. Shahabi, S. Hamidi, J.B. Ghasemi, P. Norouzi, A. Shakeri, Synthesis, experimental, quantum chemical and molecular dynamics study of carbon steel corrosion inhibition effect of two Schiff bases in HCl solution, J. Mol. Liq. 285 (2019) 626–639.
[47] C. Verma, H. Lgaz, D.K. Verma, E.E. Ebenso, I. Bahadur, M.A. Quraishi, Molecular dynamics and Monte Carlo simulations as powerful tools for study of interfacial adsorption behavior of corrosion inhibitors in aqueous phase: a review, J. Mol. Liq. 260 (2018) 99–120.
[48] F.M. Donahue, K. Nobe, Theory of organic corrosion inhibitors adsorption and linear free energy relationships, J. Electrochem. Soc. 112 (1965) 886–891.
[49] M. Talari, S. Mozafari Nezhad, S.J. Alavi, M. Mohtashamipour, A. Davoodi, S. Hosseinpour, Experimental and computational chemistry studies of two imidazole-based compounds as corrosion inhibitors for mild steel in HCl solution, J. Mol. Liq. 286 (2019) 110915.